Time Course of Individual Ca^{2+} Sparks in Frog Skeletal Muscle Recorded at High Time Resolution

Alain Lacampagne, Christopher W. Ward, Michael G. Klein, and Martin F. Schneider

From the Department of Biochemistry and Molecular Biology, University of Maryland School of Medicine, Baltimore, Maryland 21201-1503

ABSTRACT Discrete Ca^{2+} release events (Ca^{2+} "sparks") were recorded in cut segments of single frog skeletal muscle fibers using a video-rate laser-scanning confocal microscope operating in line-scan mode (63 μs per line). Fibers loaded with the Ca^{2+} indicator fluo-3 were voltage clamped at a holding potential of 0 mV, briefly reprimed at −90 mV, and then strongly depolarized with a large test pulse to activate any reprimed voltage sensors. Using this high time resolution system, it was possible to record individual Ca^{2+} sparks at ~30-fold higher time resolution than previously attained. The resulting new experimental data provides a means of characterizing the time course of fluorescence during the brief (a few milliseconds) rising phase of a spark, which was not possible with the previously used 1.5–2 ms per line confocal systems. Analysis of the time course of individual identified events indicates that fluorescence begins to rise rather abruptly at the start of the spark, continues to rise at a slightly decreasing rate to a relatively sharp peak, and then declines along a quasi-exponential time course. The mean rise time of 198 sparks was 4.7 ± 0.1 ms, and there was no correlation between rise time and peak amplitude. Average sparks constructed by temporally and spatially superimposing and summing groups of individual sparks having similar rise times gave a lower noise representation of the sparks, consistent with the time course of individual events. In theory, the rising phase of a spark provides a lower bound estimation of the time that Ca^{2+} ions are being released by the sarcoplasmic reticulum Ca^{2+} channel(s) generating the spark. The observed time course of fluorescence suggests that the Ca^{2+} release underlying a spark could continue at a fairly constant rate throughout the rising phase of the spark, and then stop rather abruptly at the time of the peak.

KEY WORDS: confocal microscopy • video-rate line-scan imaging • excitation–contraction coupling • ryanodine receptor

INTRODUCTION

Spontaneous, highly localized elevations of Ca^{2+} indicator fluorescence, termed Ca^{2+} "sparks," were first detected in confocal microscope images of rat cardiac myocytes studied under resting conditions (Cheng et al., 1993). Similar events were subsequently detected in resting skeletal muscle fibers (Klein et al., 1996). Ca^{2+} sparks occur at increased rates during small depolarizations of both cardiac myocytes (Cannell et al., 1994, 1995; Lopez-Lopez et al., 1994) and skeletal muscle fibers (Tsugorka et al., 1995; Klein et al., 1996), leading to the idea that the macroscopic [Ca^{2+}] transient during larger depolarizations might be due to the spatiotemporal summation of many such Ca^{2+} sparks occurring at high frequencies throughout the cell. Since individual Ca^{2+} sparks are likely to result from the release of Ca^{2+} from a small localized cluster of sarcoplasmic reticulum (SR)[1] Ca^{2+} release channels, or perhaps even from a single SR channel, it is of considerable interest to characterize the kinetics of the sparks to obtain information regarding possible channel activity underlying these events.

Under conditions of very low levels of activation of Ca^{2+} release in skeletal muscle, achieved by using either very small voltage-clamp depolarizations in fully polarized fibers (Tsugorka et al., 1995; Klein et al., 1996) or large depolarizations applied after brief repolarization of chronically depolarized fibers (Lacampagne et al., 1996), it has been possible to resolve Ca^{2+} sparks restricted to individual triads during muscle fiber depolarization. These discrete events activated by fiber depolarization are presumably initiated by voltage sensors in the transverse tubule membrane (Schneider and Chandler, 1973; Tanabe et al., 1987). In addition, very similar events can also be initiated by ligand modulation of SR Ca^{2+} release channel activity in chronically depolarized skeletal muscle fibers in which the voltage sensors for Ca^{2+} release are inactivated (Klein et al., 1996; Lacampagne et al., 1998).

The detailed examination of the properties of individual Ca^{2+} sparks constitutes an important new means of investigating mechanisms underlying elevation of myoplasmic [Ca^{2+}] during physiological activation of

Address correspondence to Dr. Martin F. Schneider, Department of Biochemistry and Molecular Biology, University of Maryland School of Medicine, 108 North Greene Street, Baltimore, MD 21201-1503. Fax: 410-706-8297; E-mail: mschneid@umaryland.edu

[1]*Abbreviation used in this paper:* SR, sarcoplasmic reticulum.

skeletal muscle. The duration of the rising phase of a Ca^{2+} spark provides a lower-bound estimation of the time of Ca^{2+} release from the channel or channels generating the spark, and the time course of the rising phase may provide information concerning the degree of synchrony of possible multiple channels generating the spark. For example, stepwise changes in the rising phase of a spark could indicate the sequential opening of several channels in the generation of the spark. Thus, the time course of the rising phase of a spark is an important property related to the Ca^{2+} release underlying the spark. With this in mind, all previous studies of Ca^{2+} sparks in skeletal muscle have used laser scanning confocal microscope systems with galvanometer mirrors that scan the sample at rates of 1.5–2 ms per line, and thus provide measurements at only two or three time points during the rising phase of a typical Ca^{2+} spark, which is clearly insufficient to resolve details of the kinetics of the rising phase of the spark. It is thus of great importance to record Ca^{2+} sparks at a higher time resolution then previously used in order to obtain accurate measurements of event rise times, and to examine possible details of the time course of the rising phase of the Ca^{2+} sparks.

We have now used a laser-scanning confocal system based on a resonant galvanometer that provides video-rate scanning (Tsien and Bacskai, 1995) to obtain line scan images of Ca^{2+} sparks in skeletal muscle fibers 32-fold higher in time resolution than previously available using 2 ms/line confocal systems. Using this high speed system, we have been able to resolve details of the rising phase of individual voltage-activated Ca^{2+} sparks during large depolarizations applied after brief repriming in chronically depolarized fibers. Our results indicate that the rising phase of the Ca^{2+} sparks exhibits an abrupt onset and relatively rapid attainment of near maximal rate of rise, a slightly but continuously decreasing rate of rise during the rising phase and a sharp peak at the transition from the rising to the falling phase of the spark. These observations would be consistent with an abrupt turn on of Ca^{2+} release from the SR channel(s) generating the spark at the start of the rising phase of each Ca^{2+} spark, a relatively constant rate of release of Ca^{2+} throughout the rising phase of the spark and an abrupt turn off of release from the channel(s) at the end of the rising phase of each spark.

METHODS

Cut segments of single *ileofibularis* muscle fibers from frogs (*Rana pipiens*) were manually isolated in a Ca^{2+}-free, high-K^+ relaxing solution and mounted in a double Vaseline gap chamber, as previously described (Kovacs et al., 1983; Klein et al., 1996; Schneider and Klein, 1996). In brief, single fiber segments were transferred to a double Vaseline gap chamber, mounted under stretch close to the microscope cover glass floor (3.6–4.0-μm sarcomere length), and Vaseline seals were formed. Fibers were then mechanically notched close to the Vaseline seal at each endpool segment and equilibrated with a standard internal solution at the endpools containing (mM): 80 K^+ glutamate, 5.5 $MgCl_2$, 5 Na_2ATP, 4.5 Na^+ Tris maleate, 13.2 K^+ Tris maleate, 0.1 EGTA, 0.008 $CaCl_2$, 20 phosphocreatine (disodium salt), 5 glucose, pH 7.0, and 50 μM fluo-3. The middle pool was changed to an "external" solution containing 125 tetraethylammonium-methanesulfate, 5 K^+-HEPES, 2 $CaCl_2$, and 3×10^{-4} TTX, pH 7.0. All experiments were conducted at room temperature (20–23°C).

The fiber chamber was mounted on an inverted microscope (Diaphot 300 with a PlanApo 60× 1.4 NA oil objective; Nikon Inc.) and fiber fluorescence was imaged with a RCM-8000 video-rate confocal system operated in line-scan (x vs. t) mode (Nikon Inc.). This system scanned a 108-μm line along the length of a fiber in 63 μs, resulting in a full x vs. t image (512 × 480 pixels) in ~30 ms. Optical resolution of specimens in air on this system was determined to be 0.3 μm in the x and y dimensions, and 0.8 μm in the z (vertical) dimension, based on the imaging of subresolution fluorescent beads adhered to a coverslip in air (full-width half-maximum determination).

Fibers were voltage-clamped and held at 0 mV for a minimum of 30 s before the experimental protocol that allowed for full inactivation of the voltage sensors. Fibers were then stepped to −90 mV for varying durations, allowing a small fraction of the total voltage sensor population to reprime (Lacampagne et al., 1996). After this brief repriming period, a strong test pulse depolarization to +40 mV elicited Ca^{2+} release from the SR channels controlled by the fraction of reprimed voltage sensors. During each pulse protocol, five successive line-scan images were acquired, representing two frames before the test pulse, two during the pulse (60 ms), and one frame after the termination of the pulse. A maximum of five such sequences were carried out at a given scan location to prevent damage of the preparation due to laser illumination. For example, in 17 runs from five fibers, the average number of sparks identified during the test pulses of the first and fifth sequences were 2.1 ± 0.5 and 1.5 ± 0.4, respectively. This difference is not statistically significant ($P > 0.38$). All imaging was performed while focused a minimal distance into the fiber myoplasm to minimize refractive index mismatch and the consequent deterioration of resolution (Hell et al., 1993).

The amplitude of the fluorescence signal obtained with a fluorescent indicator dye such as fluo-3 depends on the concentrations of Ca^{2+}-dye complex and free dye, which in turn depends on the local $[Ca^{2+}]$ level at each location in the fiber, the kinetics of the Ca^{2+}-dye reaction and the diffusion of free Ca^{2+}, Ca^{2+}-dye, and free dye in the fiber. To partially compensate for the effects of dye concentration, the fluorescence line scan images were routinely converted to images of $\Delta F/F$, where F is the average fluorescence at any spatial location during a reference period before application of a depolarizing pulse, and ΔF is the difference between time-dependent changes of F and the average value of F within the line-scan image. For the present experiments, the average value of F was calculated as average spatial distribution of fluorescence along the scan line during the two images before the start of the depolarizing test pulse, when the fiber was at −90 mV.

Event selection criteria were as described previously for experiments with laser scan rates of 2 ms per line (Lacampagne et al., 1996; Klein et al., 1997). Initially, the five video rate frames (63 μs/line) from each pulse protocol were temporally compressed to an equivalent time scale of 2 ms/line (e.g., Fig. 1 B) and displayed as a $\Delta F/F$ image. A rectangular box (3.9 μm × 20 ms) was then superimposed over each putative event and the time course and spatial width of the fluorescence in the rectangle were assessed for acceptance criteria: $\Delta F/F$ amplitude ≥0.4, half duration >6 ms, and half width >0.7 μm. Additionally, events were accepted only if they were visually determined to be nonoverlap-

ping, and within the test pulse interval. After the event-selection process, the spatial and temporal coordinates of the identified events were used to extract "strip" images (50 spatial pixels, or 11 μm) for subsequent analysis and display.

RESULTS

Video-Rate Recording of Ca^{2+} Sparks

Fig. 1 A presents four successive video-rate line-scan fluorescence (*F*) images recorded starting 1.3 s after repolarizing the fiber to −90 mV from the holding potential of 0 mV. Each image consists of the fluorescence detected at 512 successive spatial locations (vertical in image) during 480 successive scans along the same line in the fiber, acquired at 63-μs intervals, to create a line-scan image of fluorescence as a function of position (vertical) and time (horizontal). A gap between successive images, indicated by vertical black bars in Fig. 1 A, corresponds to the vertical flyback time of ~3 ms between successive video image frames, during which line scan data were not acquired by the confocal system. After each gap, the next image was continuously acquired at 63 μs/line.

The first (left-most) video-rate line scan image in Fig. 1 A was recorded during the final 30 ms of the repriming interval, during which the fiber membrane potential was stepped to −90 mV to restore a small fraction of voltage sensors from the state of inactivation produced by the 0-mV holding potential used in these experiments (Fig. 1, top). As shown by the rather uniform fluorescence in the first video rate line scan image frame (Fig. 1 A), no detectable release event activity was observed during the repriming interval. Beginning 2 ms after the start of the second line scan image frame in Fig. 1 A, the voltage clamp command was stepped from −90 to +40 mV (top) and this depolarization was maintained for the remainder of the second video frame (28 ms) and for 29 ms of the third frame. During the depolarization, the fluorescence in the fiber was increased as expected, since any voltage sensors restored during the preceding repriming interval should be activated during the large depolarization, and conse-

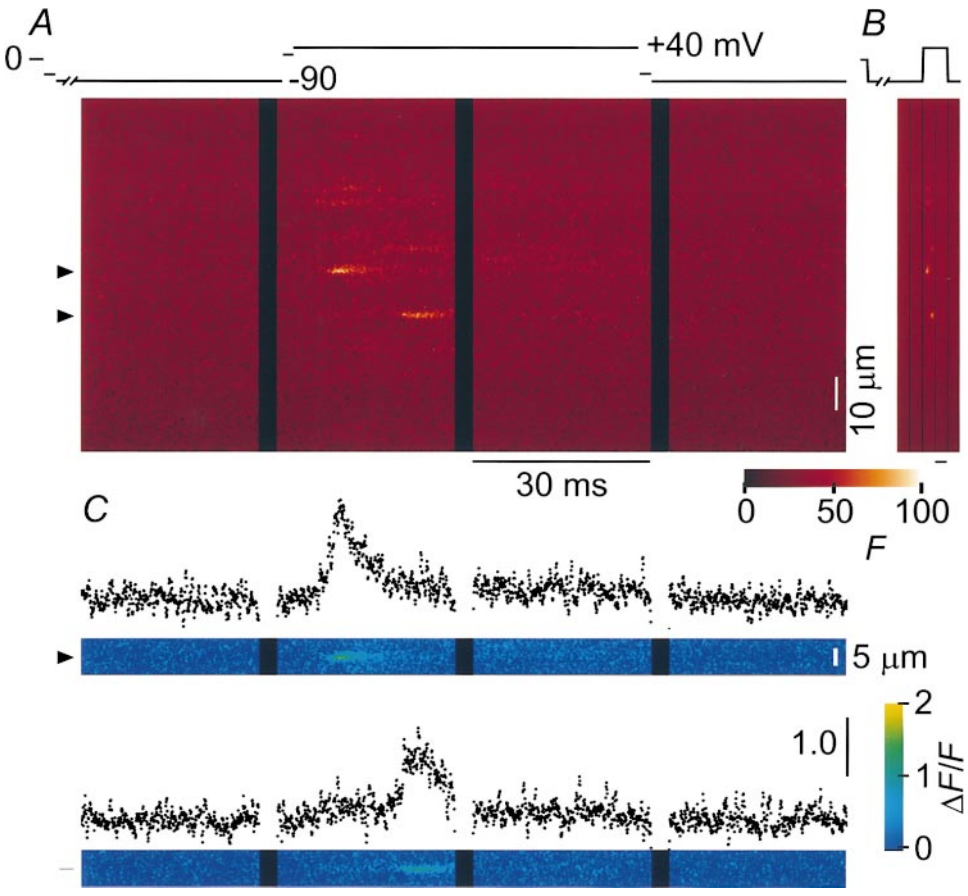

FIGURE 1. Video-rate confocal imaging of Ca^{2+} sparks. (A) Four successive video-rate line-scan images exhibiting discrete localized Ca^{2+}-release events (Ca^{2+} sparks). The fiber was reprimed at −90 mV for 1.3 s, stepped to a test potential of +40 mV for 60 ms, and then returned to −90 mV. The sequence of four images includes the end of the repriming interval (first panel), the test pulse (second and third panels), and 30 ms after the termination of the test pulse (fourth panel). The voltage time course is shown diagrammatically above the image. Black bars between the successive images represent the vertical flyback interval between video frames (3 ms), during which fluorescence recording was blanked. (B) The sequence of four video-rate images in A, plus another image of the sequence (not shown), compressed 32-fold in time to the equivalent of a laser scan rate of 2 ms per line. Both A and B are displayed in units of absolute fluorescence (*F*). (C) Two $\Delta F/F$ strip images from A that represent individual triads exhibiting Ca^{2+} sparks during the test depolarization. Above each strip image is the time course of fluorescence ($\Delta F/F$) calculated as the average of seven pixels (1.5 μm) at the spatial center of the image.

quently initiate SR Ca^{2+} release activity. As previously reported using lower time resolution line-scan imaging (Lacampagne et al., 1996; Klein et al., 1997), the fluorescence line-scan image recorded during depolarization of such briefly reprimed fibers exhibits a pattern of highly localized, discrete elevations of fluorescence (Ca^{2+} sparks), each presumably generated by the release of Ca^{2+} from a single SR Ca^{2+}-release channel, or perhaps by a small cluster of such channels. However, in contrast to previous lower time resolution line scan images, in which Ca^{2+} sparks have a somewhat spot-like shape, the discrete Ca^{2+} release events recorded at video rate line scan time resolution in Fig. 1 A have a "comet-like" appearance due to the recording of 32-fold more scans of the same line within a given time interval.

1 ms before the end of the third video-rate line scan frame in Fig. 1 A, the command voltage was stepped back to −90 mV, which returned any reprimed voltage sensors to the resting state and thus halted voltage-activated Ca^{2+} release. Finally, the voltage was stepped back to the initial holding potential of 0 mV (not shown) for at least 30 s to inactivate any voltage sensors that were reprimed during the preceding run, before beginning the next run. Note that an additional video-rate line scan image frame (not shown in Fig. 1 A), which ended 3 ms before the start of the first frame shown in Fig. 1 A, was also recorded with the fiber held at −90 mV during the repriming period before the depolarizing test pulse and was used for calculating the resting fluorescence distribution along the scan line.

The membrane potential time course during the acquisition sequence is shown above the four fluorescence line-scan images in Fig. 1 A. In these experiments, the membrane voltage and current were recorded simultaneously with the line-scan images, but at a sampling rate of 2 ms per point. The sampling interval of each point of the membrane current and voltage records corresponds to ~32 lines of the line-scan images, so the data points of the voltage records shown here appear as contiguous 2-ms segments.

High Temporal Resolution Time Course of Ca^{2+} Sparks

The comet-like local fluorescence changes recorded here using video-rate confocal line-scan imaging correspond to the same discrete release events as those that underlie the Ca^{2+} sparks recorded previously with lower speed confocal line scan systems. This can be demonstrated by temporally "compressing" the present high time resolution image in Fig. 1 A by averaging the fluorescence at each spatial location in each successive group of 32 sequential lines in Fig. 1 A. This temporal compression results in an image (Fig. 1 B), in which each line corresponds to 2 ms, as in our earlier 2-ms/line resolution images (Klein et al., 1996; Schneider and Klein, 1996). The resulting image, which was constructed from the high time resolution images in Fig. 1 A plus the additional video-rate image recorded just before those in Fig. 1 A, exhibits Ca^{2+} sparks with spatio-temporal distributions closely resembling those reported for previous 2-ms/line acquisition systems. Note that the vertical black lines in Fig. 1 B correspond to the 3-ms gaps between images in Fig. 1 A.

Fig. 1 C displays two $\Delta F/F$ strip images from two regions where individual triads (Fig. 1 A, arrowheads) exhibited elevations of fluorescence, indicating the occurrence of discrete release events originating at these triads. The fluorescence distribution resulting from the release events was spatially localized to the individual triads (not shown), as found previously with lower time-resolution recording. The records above each strip image in Fig. 1 C present the time course of $\Delta F/F$ obtained by averaging the time courses recorded in the central seven pixels (1.5 μm) in each strip image. In contrast to previously recorded spark time courses, which exhibited only about two to four points during the rising phase of a spark, the present video-rate system provides a relatively large number of determinations of $\Delta F/F$ during the rising phase of each spark, and an even larger number of points during the slower falling phase. Thus, the present recordings provide a previously unavailable degree of time resolution for characterizing the time course of fluorescence during the Ca^{2+} sparks. However, due to the presence of gaps in the recording, as seen during the falling phase of the spark for the lower strip in Fig. 1 C, the detailed analysis of the spark time courses must be restricted to sparks such as that shown in Fig. 1 C (top), in which most of the time course of the event falls within a given image. This restriction was not difficult to satisfy since the half duration of the events is well under the 30-ms duration of a single image frame of the present recording system (below).

Mathematical Description of Time Course of Observed Ca^{2+} Sparks

The high temporal acquisition rate of the RCM-8000 confocal system necessarily implies that the pixel dwell time is brief, and therefore the average number of detected photons per pixel is low. These conditions require that the photomultiplier tube gain be increased above the setting for optimal signal-to-noise during acquisition. Consequently, the images acquired using this system are considerably noisier than images and analysis described in our earlier publications using a slower confocal line-scan acquisition system. The statistical nature of the appearance of Ca^{2+} sparks in our line-scan images within different triads and at different times during the test depolarization prevents us from simply averaging multiple frames to decrease the noise associ-

ated with any individual spark. Thus, to establish the time of occurrence of each spark, as well as to extract parameters of individual sparks, we have characterized the time course of $\Delta F/F$ by fitting each record to a function that reproduces the main features of the observed time course.

Fig. 2 presents an analysis of the time course of the upper spark in Fig. 1 C, now presented on the same expanded time scale in Fig. 2, A and B. The solid line in Fig. 2 A gives the least squares fit of the function

$$\Delta F/F = C \quad (t \le d_1)$$

$$\Delta F/F = A\{1 - \exp[-k_1(t - d_1)]\} \exp[-k_2(t - d_2)] + C \quad (t > d_1) \qquad (1)$$

to the experimental record starting at the beginning of the second frame and continuing to the end of the depolarizing pulse. The values of the parameters A, k_1, d_1, k_2, d_2, and C were adjusted to give a best least squares fit of Fn. 1 to the experimental record. The fit to the experimental record in Fig. 2 A succeeds in locating the start (d_1) of the rising phase of the Ca^{2+} spark. However, the fit of Fn. 1, which provides a function with a continuous rate of change (i.e., continuous derivative) at all times after the start of the spark at $t = d_1$, fails to fully reproduce the sharp peak with apparently discontinuous slope exhibited by the experimental record. This failure of Fn. 1 to fully reproduce the sharp peaks of many experimental Ca^{2+} spark time courses was a systematic observation (see below).

Fig. 2 B presents the same experimental Ca^{2+} spark $\Delta F/F$ time course as in Fig. 2 A, but now fit by the function

$$\Delta F/F = 0 \quad (t \le d_1)$$

$$\Delta F/F = A\{1 - \exp[-k_1(t - d_1)]\} \quad (d_1 < t \le d_2) \qquad (2)$$

$$\Delta F/F = A\{1 - \exp[-k_1(d_2 - d_1)]\} \exp[-k_2(t - d_2)] + C \quad (t > d_2)$$

over the same interval as used in Fig. 1 A. The values of the parameters A, k_1, d_1, k_2, d_2, and C were adjusted to give a best least-squares fit of Fn. 2 to the experimental record. The resulting fit of Fn. 2, which has discontinuous derivatives at both its start and peak, closely follows all aspects of the experimental record in Fig. 2 and provides a better reproduction of the sharp peak in the experimental record in Fig. 2 than could be achieved using the function in Fn. 1.

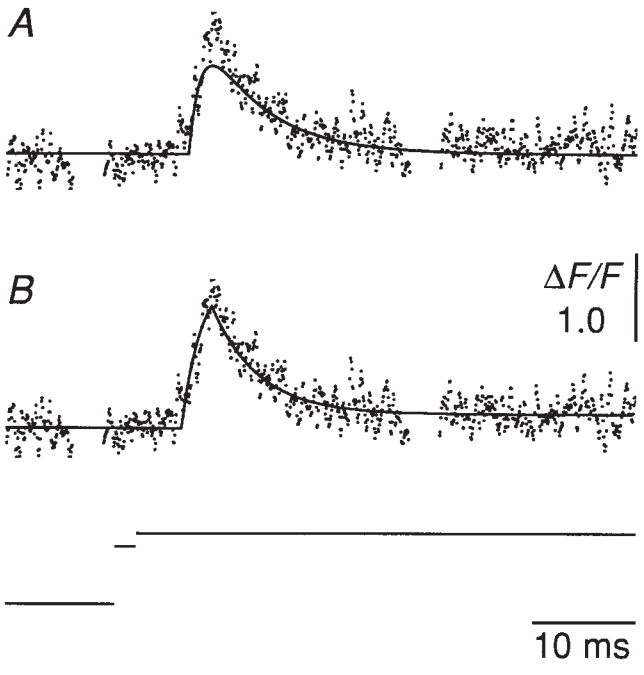

FIGURE 2. The time course of $\Delta F/F$ during Ca^{2+} sparks. The data record is the $\Delta F/F$ time course during the latter part of the repriming interval, and the first 44 ms of the 60-ms test depolarization, from Fig. 1 C (top). The vertical flyback intervals between video frames are shown as gaps in the data record. The depolarizing command pulse begins 10 ms after the start of the record segment and extends 4 ms beyond it. In A, the record is shown with a fit of Fn. 1 (see RESULTS) superimposed. In B, the same record is fit by Fn. 2. The membrane voltage is shown diagrammatically at bottom.

A Sequence of Two Exponentials Systematically Describes the Ca^{2+} Spark Time Course

Functions 1 and 2 were separately fit to each of 198 identified Ca^{2+} sparks recorded from 11 fibers using the repriming protocol and the present video-rate confocal line-scan system. To evaluate the goodness of the fits of Fns. 1 and 2 to this group, we constructed the residuals for each fit as the time course of the experimental record for each spark minus the fit to that record.

The upper record in Fig. 3 A presents the average of the residual differences between each experimental record and its fit by the function in Fn. 1, with the residuals synchronized at the time of the start of the rising phase of the fit to each observed spark (d_1 in Fn. 1; indicated by ▼ and the first vertical dashed line in Fig. 3). The second vertical dashed line indicates the mean time of the peak of the fits of Fn. 1. The mean residual record synchronized at d_1 exhibits a series of sequential positive and negative deviations from zero. The fits of Fn. 1 thus systematically fell sequentially below and above the data, indicating that the failure of Fn. 1 to reproduce the individual experimental Ca^{2+} spark record in Fig. 2 was a systematic finding over the population of 198 sparks identified in this study. The lower record in Fig. 3 A and in all other panels of Fig. 3 indicates the number of records contributing to the average residual at each point in time. This value decreases from the full number of 198 observed sparks at times when portions of one or more records fall within the flyback time between successive video frames (above).

The upper record in Fig. 3 B presents the average residuals for the fit of Fn. 2 to the records of 198 identified Ca^{2+} sparks, with the residuals synchronized at the time of the start of the spark rising phase of each spark fit to each experimental record (d_1 in Fn. 2; indicated by ▼ and the first vertical dashed line). The second vertical dashed line corresponds to the mean time of the peak (d_2) of the fits by Fn. 2. In contrast to the relatively large sequential systematic deviations of the residuals seen in Fig. 3 A, the average residual record in Fig. 3 B exhibits only a relatively brief systematic deviation between the experimental records and their fits by Fn. 2, indicating that Fn. 2 systematically provides a rather good representation of the observed spark time courses, including the sharp transition between increasing and decreasing fluorescence at the peak of the observed Ca^{2+}-spark time course.

Since the observed sparks exhibited a range of rise times (see below), the average of the residuals synchronized at the time of the start of each spark (d_1) as in Fig. 3, A and B, cannot also be perfectly synchronized at the time of the peak of the fits to the sparks. Thus, to look for possible systematic deviations between the experimental records and their fits at the time of the peaks of the sparks, we also synchronized the residuals at the time of the peak of each fit, and then averaged the residuals. For Fn. 1, the resulting average residuals synchronized at the peak of the sparks (Fig. 3 C) exhibited large, systematic deviations from the experimental records. In contrast, there was little systematic deviation between the experimental records and their fits by Fn. 2 when the residuals were synchronized at the time of the peak of the fit (Fig. 3 D). Thus, Fn. 2 closely reproduced essentially the entire time course of the observed sparks, whereas Fn. 1 could not accurately reproduce the time course of the observed sparks. Consequently, the fit to Fn. 1 was used only to provide starting values for the fit to Fn. 2, particularly the d_1 variable. All later consideration of properties of individual sparks in this paper, as well as all synchronization of individual experimental records carried out here, used parameter values obtained from the fit of Fn. 2 to the experimental records.

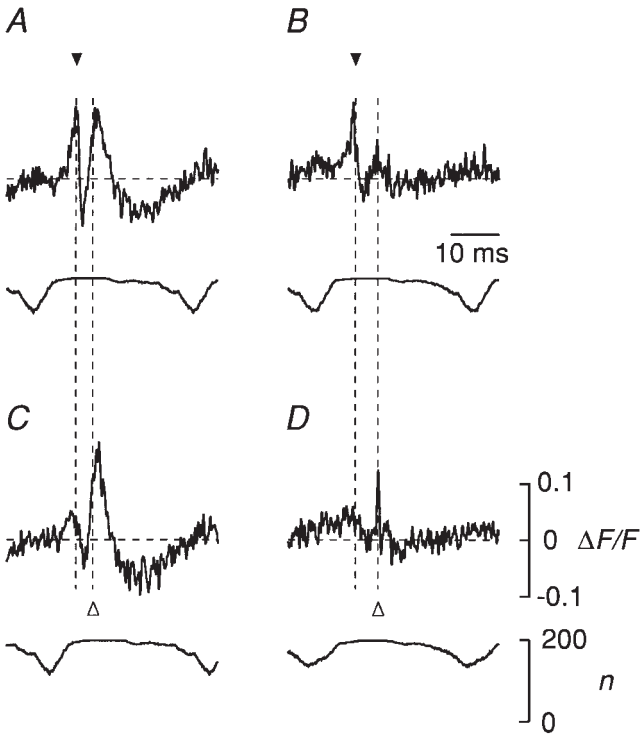

FIGURE 3. Analysis of residuals of fits to the data records. Residuals of the least squares fits to the $\Delta F/F$ time course of each spark ($n = 198$) were calculated as the difference between the data and the fit of either Fn. 1 (A and C) or 2 (B and D) to the data. The residuals of each record were then aligned at the time of the start (A and B) or peak (C and D) of the corresponding fit, and summed. The sum of residual records for each condition was then divided by a template (bottom of each panel) that was formed by aligning and summing a binary mask in a manner identical to a corresponding data record. The template corrected for the variable number of nonzero data elements at each time point of the sum, due to presence of gaps in the individual data records and the different amounts of shifting required to align each record. The vertical scales in D also apply to A–C.

Spark Rise Times and Amplitudes

The amplitude of each spark was obtained by averaging seven values around the time of the peak of the fit of Fn. 2 to the time course of $\Delta F/F$, and the rise time of each spark was determined as $d_2 - d_1$ from the fit of Fn. 2. The resulting spark amplitudes and rise times varied considerably within the same line scan image, as well as between images within a given fiber, as was previously observed using lower time resolution line-scan images. Fig. 4 A presents a histogram of the rise times of the 198 individual sparks monitored in this study. The line in Fig. 4 A represents a single exponential fit to the rise time histogram, including all events having rise times >3.8 ms, to avoid regions of the histogram where we may have possibly failed to detect some events due to brief rise times. The time constant of the fit, 2.5 ms, would correspond to the mean channel open time if the identified sparks were generated by the opening of a single two-state channel. The average rise time of all identified events was 4.7 ± 0.1 ms, which is much larger than the predicted value of 2.5 ms due at least in part to our presumed inability to detect events generated by very brief openings.

Fig. 4 B presents the relationship between the rise time and amplitude of each spark. The data indicate that the amplitude of each spark was not correlated with its rise time ($P > 0.93$), as previously observed using lower time resolution recording (Klein et al., 1997). As was the case in previous analyses, Fig. 4 B includes all of the relatively larger amplitude events occurring in

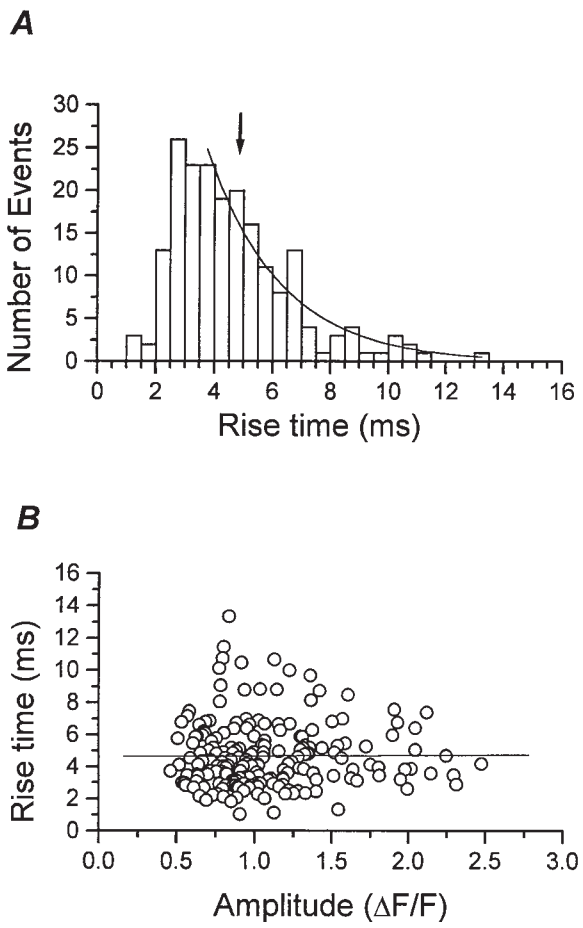

FIGURE 4. The rise times of individual Ca^{2+} sparks. Rise times were determined as the difference between the time of the peak (d_2; Fn. 2) and the start of the rising phase of the spark fit (d_1; Fn. 2). (A) The rise time distribution >3.8 ms was fit to a single exponential function that yielded a time constant of 2.5 ms and an estimated error of ±0.3 ms. The arrow indicates the mean of the distribution, 4.7 ± 0.2 ms. (B) The amplitude of each spark is plotted against its rise time value. Peak amplitudes were determined as the average of seven points around the time of the peak of the fit of Fn. 2 to each record. There was no correlation between the rise time of the spark and its amplitude ($P > 0.93$).

the images for this study since larger amplitude sparks can be unambiguously identified. However, the population of sparks represented in Fig. 4 B is truncated at the sampling cut-off amplitude of $\Delta F/F = 0.4$, so the rise time versus amplitude relationship at lower amplitudes is not represented in Fig. 4 B.

Time Courses of the Largest Amplitude Sparks

Computer simulations of the formation of Ca^{2+} sparks demonstrate that the observed amplitude of the Ca^{2+}-dye distribution resulting from a point source of Ca^{2+} release exhibits a maximum amplitude when the confocal scan line passes exactly through the release source, and decreases monotonically as the scan line passes further from the release site (Pratusevich and Balke, 1996; Jiang et al., 1998). Thus, on average, the largest recorded sparks should correspond to the situation of the scan line passing relatively close to the release source, and whose waveform would be least affected by diffusional delays. Fig. 5 A presents strip images of a subset of 6 of the largest 14 sparks observed in these experiments, in units of $\Delta F/F$, recorded in five different fibers. The time course of the Ca^{2+} spark at the center of each strip is shown above the corresponding strip. The best fit of Fn. 2 is shown superimposed on each time course and provides a rather close fit to each of the experimental records in Fig. 5, including the sharp peaks.

Fig. 5 B shows the average time course calculated using the 14 largest amplitude sparks identified in this study, including the six sparks in Fig. 5 A, and eight other sparks (not shown). These sparks are indicated in Fig. 4 B by the 14 right-most points along the abscissa. For Fig. 5 B (left), each experimental record was shifted in time so as to be synchronized at the start (d_1) of the rising phase of the fit of Fn. 2 to the record, whereas in Fig. 5 B (right) the experimental records were synchronized at the time of peak (d_2) of the fit. These average records clearly demonstrate a sharp transition to a near maximal rate of rise early in the average record calculated by synchronizing at the start (left), and a sharp transition from rising to falling phases at the peak of the average synchronized at the time of peak (right). However, these largest events, averaged in Fig. 5 B, represent a fairly wide range of spark rise times (2.5–6.8 ms) so that when these events are synchronized at the start, the peaks are not synchronized, and vice versa for synchronization at the peak, thus accounting for the difference in the two averaged records in Fig. 5 B. To obtain better estimates of the entire average time course of a subpopulation of events, independent of the point at which they are aligned, it is necessary to average events with similar rise times.

Average Time Courses for Sparks of Similar Rise Times

Fig. 6 presents time courses and strip images for the averages of three subpopulations of sparks having relatively narrow ranges of rise times: (A) 13 sparks with rise times between 2.0 and 2.5 ms, (B) 18 sparks with rise times between 4.4 and 4.9 ms, and (C) 19 sparks with rise times between 6.2 and 6.9 ms. In each group, the sparks were shifted in time so as to be synchronized at the start of the rising phase before averaging. Because of the relatively narrow range of rise times of the events in each group, each of the average time courses synchronized at the start of the spark in Fig. 6 is also almost in synchrony at its peak (i.e., individual records making up the average have times of peak within 0.35 ms of the average time of peak). The average sparks in Fig. 6 thus present an accurate representation of the entire time course of the individual events within each

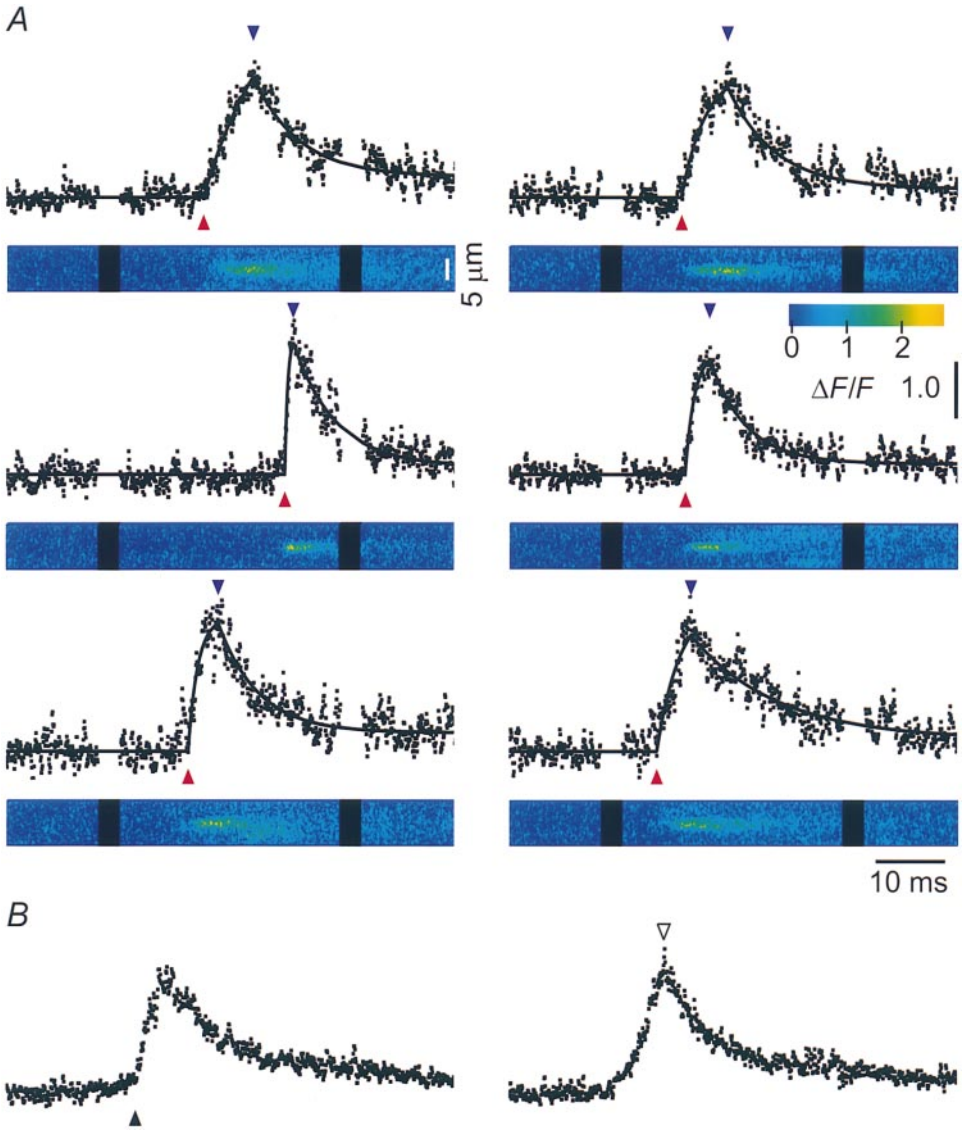

FIGURE 5. Images and time courses of largest amplitude sparks. (A) A subset of 6 of the 14 largest sparks of this study, as determined by the peak of the fit to Fn. 2, are shown as image strips and corresponding $\Delta F/F$ records. Superimposed on each time course is the fit of Fn. 2. Arrowheads indicate the temporal position of the start of the spark (red) and the peak (blue) as determined from the fit. (B) The $\Delta F/F$ records of the largest amplitude sparks ($n = 14$; 2.1 ± 0.1 $\Delta F/F$) were temporally shifted to the time of the start of the fit spark (d_1, ▲) and time of the peak fit (d_2, ▽), respectively, and averaged.

group since both the start and peak times of the individual records making up the average are nearly synchronized. These average sparks also show the general features of individual sparks (e.g., Figs. 1 and 5), namely, relatively sharp transitions at the start and peak of sparks and a quasi-exponential decline from the peak.

It is important to note, in connection with the calculation of the average sparks shown in Figs. 5 B and 6, that the sharp transitions observed in these records at the start and peak of the spark were not artifactually introduced by the fitting and alignment procedure. For example, it might be argued that locating the peaks of individual spark records (e.g., Fig. 5 A) by fitting them to Fn. 2 might be susceptible to noise in the record, so that when several such records are aligned at this point and averaged, the resulting average record will have a sharp peak where there was none in the individual records. We tested this possibility using the fit of Fn. 1 to each spark record used in Fig. 5 B. Note that all of the fits of this function to single spark records exhibited a rounded peak (e.g., Fig. 2 A). Poisson-distributed random noise was added to each fit record to simulate photomultiplier tube noise. The resulting records were fit to Fn. 2, aligned at the time of the peak and averaged, in a manner identical to the formation of the record in Fig. 5 B (right). The resulting average record also exhibited a rounded peak (not shown), demonstrating that a sharp peak was not introduced into the average spark by the analysis procedure. This was true even when the variance of the added Poisson noise was 50% greater than the experimentally measured noise.

We also tested whether the form of the fitting function influenced the degree to which the average spark records exhibited sharp transitions. The same 14 records used in the analysis above were fitted to a gaus-

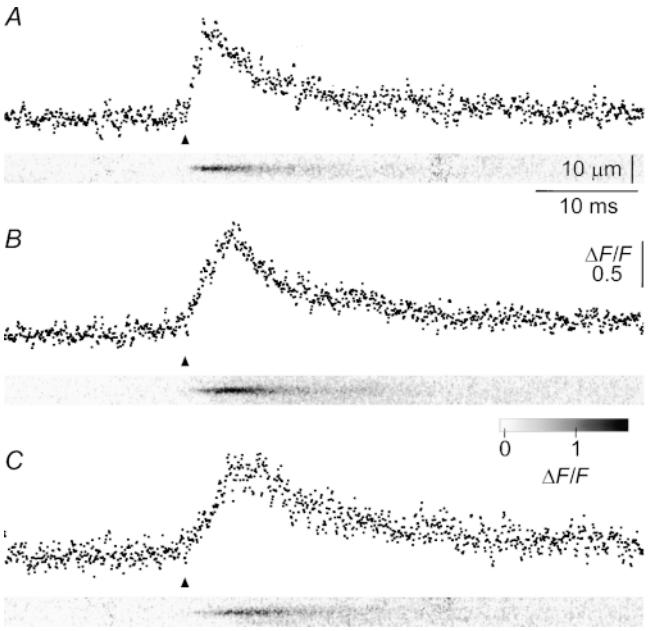

FIGURE 6. Construction of average sparks having similar rise times. Average sparks consisting of various subsets of the 198 identified sparks were formed by aligning each spark record at the beginning of the rising phase of the spark fit (d_1; Fn. 2) to the $\Delta F/F$ time course (▲). (A) Average of 13 sparks having rise times between 2.0 and 2.5 ms. (B) Average of 18 sparks with rise times between 4.4 and 4.9 ms. (C) Average of 19 sparks with rise times between 6.2 and 6.9 ms. Each panel shows the resulting average strip image below, and the corresponding $\Delta F/F$ time-course record above. Rise times were calculated as the time between the peak (d_2) and start (d_1) of the spark fit by Fn. 2.

sian function, a function whose derivative is everywhere continuous. Average spark records were formed by aligning and averaging the individual spark records at either (a) the time of the mean of the gaussian fit, (b) the time of the mean − 1 SD of the fit, or (c) the mean + 1 SD. The averages resulting from the first and second procedures were very similar to the averages shown in Fig. 5 B, left and right, respectively. The first showed a sharp transition at the time of the peak of the average spark, which occurred slightly earlier than the time of the mean of the fit. The second showed a sharp transition at the start of the average spark, which was slightly broader than the corresponding average in Fig. 5 B. The third procedure, which was equivalent to aligning each individual spark record at a point on its falling phase, resulted in an average spark of much lower amplitude and broader waveform. Thus, the sharp transitions in the average sparks of Figs. 5 B and 6 were not introduced by noise in the individual spark records, or by the form of the fitting function, and are thus characteristic features of the individual sparks as well.

Rate of Rise and Decay Time Constant of the Sparks

The average time courses for the sparks having three different ranges of rise times (Fig. 6) indicate that the slope of the rising phase of the average spark appears to decrease with increasing rise time. This observation is consistent with the observed lack of correlation between spark amplitude and spark rise time (Fig. 4). If shorter and longer rise time events reach the same average peak amplitude, then the longer rise time events must exhibit a lower average rate of rise than the shorter rise time events. Table I gives the spark parameters calculated as the mean values of the individual sparks within the group indicated in the first column, with the number of sparks within that group given in the second column. From Table I, the initial rate of rise (fifth column), obtained as $A \cdot k_1$ from the fit of Fn. 2 to each spark, decreased as the spark rise time increased (fourth column). In contrast, the time constant of the declining phase of $\Delta F/F$ in a spark (Table I, column six), obtained from the fit of Fn. 2 as $1/k_2$, was independent of spark rise time.

Table I also gives the average values of the amplitude and rise time for all sparks in this study, and for each of the three groups of sparks in Fig. 6, as well as for the group of the 14 largest sparks (average time course in Fig. 5 B). The amplitude values correspond to the average of seven time points centered at the time of peak,

TABLE I

Average Properties of Ca^{2+} Sparks

Group	*n*	Amplitude	Rise time	Initial rate of rise	Decay time constant
		ΔF/F	*ms*	*ΔF/F·ms⁻¹*	*ms*
All events	198	1.05 ± 0.03	4.6 ± 0.1	0.7 ± 0.5	8.5 ± 0.4
Largest amplitude	14	2.07 ± 0.10‡	4.2 ± 1.7	1.6 ± 0.4	7.3 ± 0.6
Rise time 2.0–2.5 ms	13	0.98 ± 0.07	2.3 ± 0.1	1.4 ± 0.2	7.9 ± 0.8
Rise time 4.4–4.9 ms	18	1.18 ± 0.09	4.7 ± 0.1	0.6 ± 0.1	8.3 ± 0.9
Rise time 6.2–6.9 ms	19	1.15 ± 0.06	6.6 ± 0.1	0.4 ± 0.1	7.9 ± 1.1

The amplitude was determined from the experimental record as the average of seven points centered at the time of the peak of the fit of Fn. 2 to each record of $\Delta F/F$ for each spark. Using the fit of Fn. 2, the rise time is defined as $d_2 - d_1$, the time of the start of the spark, and its peak; the initial rate of rise as $A \cdot k_1$ (see Fn. 2) and the decay time constant of the decline of each spark after the peak as $1/k_2$. All values are mean ± SEM.

as determined from the fit of Fn. 2 to each record. The other parameters in Table I are as defined above. The present estimates of spark properties can be compared with estimates of spark properties from our earlier publications, obtained using slower confocal scan rates, on skeletal muscle fibers under similar conditions. The amplitudes of sparks selected here were similar to those in previous studies of voltage-activated sparks after brief repriming in depolarized fibers (Lacampagne et al., 1996; Klein et al., 1997). A previous estimate of the mean spark rise time, taken as the 10–90% rise time of each $\Delta F/F$ time course record, was 5.6 ms (Klein et al., 1997). The corresponding mean value of the 10–90% rise time of the sparks in this study, from the time course of the fit of Fn. 2 to the present high time resolution records of $\Delta F/F$, was 3.2 ± 0.1 ms. The difference in these estimates is attributable to inadequate sampling of the rising phase of the sparks, and consequent overestimation of the rise time due to filtering of the records in the earlier study.

DISCUSSION

Ca^{2+} sparks are localized elevations of fluorescence resulting from Ca^{2+} binding to the Ca^{2+} indicator, fluo-3, present in the myoplasm. The sparks originate at single triad junctions, as expected for the location of the ryanodine receptor–SR Ca^{2+}-release channels in the SR junctional face membrane at the triads. Each spark presumably arises from the Ca^{2+} released by the opening of one SR Ca^{2+}-release channel or a small cluster of such channels located at a given triad. Thus, the properties of the observed Ca^{2+} sparks potentially provide information concerning the channel activity underlying each observed spark. Previous studies using confocal scanning rates of ~1.5–2 ms/line provided limited temporal information concerning this estimation of channel activity since the half duration of the sparks is of the order of 10 ms. The high time resolution line-scan studies of Ca^{2+} sparks reported here consequently provide new information that may be helpful in characterizing the SR Ca^{2+} channel activity underlying the observed Ca^{2+} sparks.

Theoretical Basis of Observed Ca^{2+} Spark Time Courses

The fluorescence time course of a Ca^{2+} spark observed using a laser scanning confocal microscope in line-scan mode, as in the present experiments, is determined both by the spatio-temporal spread of the concentration of fluorescent Ca^{2+}-dye complex from the channel or cluster of channels that constitutes an effective point source of Ca^{2+} release, and by the imaging of this fluorescence using the laser-scanning confocal microscope system. Several detailed models of the diffusion and binding of Ca^{2+} from a point source at the periphery of a myofibril at the triad junction, including Ca^{2+} binding to myoplasmic sites and diffusion of Ca^{2+} (Pratusevich and Balke, 1996), as well as diffusion of free dye and Ca^{2+}-dye complex (Jiang et al., 1998; Smith et al., 1998), have been developed. The resulting model confocal images of the simulated spread of fluorescence for a square-wave Ca^{2+}-release rate time course (i.e., a rate of release that jumps instantaneously from zero to a constant rate, remains constant for a few milliseconds, and then instantaneously turns off to zero) from a point source of Ca^{2+} indicates that the amplitude of the simulated spark depends strongly on the relative position of the Ca^{2+}-release site relative to the scan line. In contrast, the rise time of the simulated fluorescence signal is rather insensitive to the scan-line location relative to the release site, and consequently provides a good indication of the duration of the period during which Ca^{2+} release occurred in the simulation. It thus seems reasonable that if the rate of Ca^{2+} release underlying the Ca^{2+} sparks observed in the present high-time resolution studies in skeletal muscle fibers also followed a square-wave form, then the rise time of the sparks that we have characterized in these studies should correspond to the duration of the release process underlying the sparks. Based on these considerations, the mean spark rise time of 4.6 ms observed here would correspond to the mean duration of the Ca^{2+} release underlying the 198 Ca^{2+} sparks selected in this study. However, the mean value of the selected events could overestimate the actual mean open time due to our presumed failure to detect very brief openings, as indicated by the nonexponential shape of the observed rise-time histogram (Fig. 4). On the other hand, it remains to be rigorously established that the spark rise time as determined here represents the entire duration of Ca^{2+} release. For example, some channel activity could last longer than the measured spark rise time. Evaluating this possibility will require detailed modeling of the observed Ca^{2+} sparks.

Time Course of Ca^{2+} Sparks Indicates Abrupt Turn-On and Turn-Off of Ca^{2+} Release

Several characteristics of the Ca^{2+}-spark time courses observed here are consistent with Ca^{2+} sparks simulated by assuming a point source of Ca^{2+} release located relatively near the position of the scan line, and having a square-wave time course of rate of Ca^{2+} release (Pratusevich and Balke, 1996; Jiang et al., 1998). The individual sparks were well fitted by a function consisting of two sequential segments, an exponentially rising segment followed immediately by an exponentially falling segment. This function begins to rise and fall at maximum rates, respectively, at the start and peak of

each spark, as in the Ca^{2+} sparks simulated for a square-wave rate of Ca^{2+} release. When the experimentally observed time courses of individual sparks having closely similar rise times were temporally shifted so as to be synchronized at either the time of the start or the time of the peak of the sparks, and then averaged (Fig. 6), the resulting average exhibited an abrupt transition to a high, nearly maximal rate of rise and high, nearly maximal rate of fall, respectively, at the start and peak of the resulting average sparks. Thus, the temporal properties of the sparks observed here could be consistent with an underlying rate of Ca^{2+}-release wave form close to a square-wave time course.

It is important to note that, although the times of the start and peak of each spark used for shifting the individual experimental spark records before averaging were determined by the fit of the observed experimental data, the average consisted entirely of experimental data, with no fit data included. Furthermore, these features were not artifactually introduced into the average spark records by the fitting and alignment procedures used here. Thus, the abrupt transitions to near maximal rates of rise and fall at the start and peak of the synchronized and averaged sparks, as well as all other features of the average records, were inherent in the observed individual spark time courses.

We have made the unanticipated observations that the rate of rise of a spark is relatively smaller for sparks having relatively longer rise times (Table I), and that the spark amplitudes are uncorrelated with rise time (Fig. 4) or rate of rise. If the sparks with fast and slow rise times represent events generated by the same release time course, but viewed at different distances from the release source, then the slower events, which are viewed from further away, should be smaller in amplitude. However, as shown in Table I, this was not the case. The mean event amplitude remained unchanged in the groups of events in which the rise time varied by approximately threefold between groups. Thus, the distance of the scan line from the release source does not seem to explain the longer rise time events, and we tentatively reject the possibility that the long rise time sparks are due to very large events, greater than, say, three units of $\Delta F/F$, arising away from the scan line, because such events should occasionally be observed in focus. A possible interpretation of the observed decrease in rate of rise with increased spark rise time is that the open time(s) of channel(s) responsible for generating a spark is influenced by the amount of Ca^{2+} released. If this were the case, channels having a lower efflux rate, and thus giving sparks with a lower rate of rise, would remain open longer and thus have longer rise times, as observed. Alternatively, the rising phase might be related to propagation time along a region of sequential interacting Ca^{2+} release channels, termed a couplon (Stern et al., 1997), with relatively brief openings of individual channels in the couplon. In this case, couplons exhibiting relatively slower propagation might give rise to sparks of longer rise time, resulting in a lower rate of rise as observed.

Patterns of Channel Activity that may Underlie the Observed Sparks

Although the observed spark time courses could be consistent with an underlying release rate waveform that is relatively close to a square-wave form, the number of channels and absolute pattern of channel activity is not established by the present studies. At least three alternative possible general patterns of channel activity must be considered (Lacampagne et al., 1998). A single channel open for the duration of the rising phase of the spark would provide one possible basis for a square-wave rate of release. Simulations assuming current sources of magnitude similar to single channel currents measured in bilayers produce simulated Ca^{2+} sparks similar in amplitude to those observed experimentally (Pratusevich and Balke, 1996; Jiang, et al., 1998), indicating that a a single SR Ca^{2+}-release channel might generate the observed Ca^{2+} sparks. However, a cluster of a number of channels that all turn on and off in near synchrony (Marx et al., 1998) at the start and peak of the spark would also produce a similar underlying release wave form. Finally, a cluster of neighboring channels, each of which flickers on and off during the rising phase of the spark (but is largely inactive before the time of the foot and after the time of the peak of the spark), would also account for the observed time course. Further studies will be required to attempt to distinguish between these alternative possible patterns of channel activity in a spark. None the less, the present results are consistent with the idea that there is an abrupt turn on and turn off of release at the start and peak of each spark, respectively, and that the net rate of release of Ca^{2+} underlying each spark could be rather constant throughout the rising phase of the spark.

This work was supported by research grants from the National Science Foundation (MCB-9724045 to M.F. Schneider) and the National Institutes of Health (NIH; R01-AR44197 to M.G. Klein). A. Lacampagne was partially supported by the Melzer Foundation. C.W. Ward was partially supported by an NIH Post-Doctoral fellowship (Training Grant T32-AR07592 to the Interdisciplinary Program in Muscle Biology, University of Maryland).

Original version received 16 November 1998 and accepted version received 23 December 1998.

REFERENCES

Cannell, M.B., H. Cheng, and W.J. Lederer. 1994. Spatial non-uniformities in $[Ca^{2+}]_i$ during excitation–contraction coupling in cardiac myocytes. *Biophys. J.* 67:1942–1956.

Cannell, M.B., H. Cheng, and W.J. Lederer. 1995. The control of calcium release in heart muscle. *Science.* 268:1045–1049.

Cheng, H., W.J. Lederer, and M.B. Cannell. 1993. Calcium sparks: elementary events underlying excitation–contraction coupling in heart muscle. *Science.* 262:740–744.

Hell, S., G. Reiner, C. Cremer, and E.H.K. Stelzer. 1993. Aberrations in confocal fluorescence microscopy induced by mismatches in refractive index. *J. Microsc. (Oxf.).* 169:391–405.

Jiang, Y.-H., M.G. Klein, and M.F. Schneider. 1998. Numerical simulation of Ca^{2+} "sparks" in skeletal muscle. *Biophys. J.* 74:A269.

Klein, M.G., H. Cheng, L.F. Santana, Y.-H. Jiang, W.J. Lederer, and M.F. Schneider. 1996. Two mechanisms of quantized calcium release in skeletal muscle. *Nature.* 379:455–458.

Klein, M.G., A. Lacampagne, and M.F. Schneider. 1997. Voltage dependence of the pattern and frequency of discrete Ca^{2+} release events after brief repriming in frog skeletal muscle. *Proc. Natl. Acad. Sci. USA.* 94:11061–11066.

Kovacs, L., E. Rios, and M.F. Schneider. 1983. Measurement and modification of free calcium transients in frog skeletal muscle fibres by a metallochromic indicator dye. *J. Physiol. (Lond.).* 343: 161–196.

Lacampagne, A., M.G. Klein, and M.F. Schneider. 1998. Modulation of the frequency of spontaneous sarcoplasmic reticulum Ca^{2+} release events (Ca^{2+} sparks) by myoplasmic $[Mg^{2+}]$ in frog skeletal muscle. *J. Gen. Physiol.* 111:207–224.

Lacampagne, A., W.J. Lederer, M.F. Schneider, and M.G. Klein. 1996. Repriming and activation alter the frequency of stereotyped discrete Ca^{2+} release events in frog skeletal muscle. *J. Physiol. (Lond.).* 497:581–588.

Lopez-Lopez, J.R., P.S. Shacklock, C.W. Balke, and W.G. Wier. 1994. Local, stochastic release of Ca^{2+} in voltage-clamped rat heart cells: visualization with confocal microscopy. *J. Physiol. (Lond.).* 480:21–29.

Marx, S.O., K. Ondrias, and A.R. Marks. 1998. Coupled gating between individual skeletal muscle Ca^{2+} release channels (Ryanodine receptors). *Science.* 281:818–821.

Pratusevich, V.R., and C.W. Balke. 1996. Factors shaping the confocal image of the calcium spark in cardiac muscle cells. *Biophys. J.* 71:2942–2957.

Schneider, M.F., and W.K. Chandler. 1973. Voltage-dependent charge movement in skeletal muscle: a possible step in excitation–contraction coupling. *Nature.* 242:244–246.

Schneider, M.F., and M.G. Klein. 1996. Sarcomeric calcium sparks activated by fiber depolarization and cytosolic Ca^{2+} in skeletal muscle. *Cell Calc.* 20:123–128.

Smith, G.D, J.E. Keizer, M.D. Stern, W.J. Lederer, and H. Cheng. 1998. A simple numerical model of calcium spark formation and detection in cardiac myocytes. *Biophys. J.* 75:15–32.

Stern, M.D., G. Pizarro, and E. Rios. 1997. Local control model of excitation–contraction coupling in skeletal muscle. *J. Gen. Physiol.* 110:415–440.

Tanabe, T., K.G. Beam, J.A. Powell, and S. Numa. 1987. Restoration of excitation–contraction coupling and slow calcium current in dysgenic muscle by dihydropyridine receptor complementary DNA. *Nature.* 336:134–139.

Tsien, R.Y., and B.J. Bacskai. 1995. Video-rate confocal microscopy. *In* Handbook of Biological Confocal Microscopy. J.B. Pawley, editor. Plenum Publishing Corp., New York. 459–478.

Tsugorka, A., E. Rios, and L.A. Blatter. 1995. Imaging elementary events of calcium release in skeletal muscle cells. *Science.* 269: 1723–1726.